General and Unified Model of the Power Flow Problem in Multiterminal AC/DC Networks

Willem Lambrichts, *Student Member, IEEE,* and Mario Paolone, *Fellow, IEEE,*

***Abstract*—This paper proposes a generic and unified model of the power flow (PF) problem for multiterminal hybrid AC/DC networks. The proposed model is an extension of the standard AC-PF. The DC network is treated as an AC one and, in addition to the *Slack*, *PV* and *PQ* nodes, four new node types are introduced to model the DC buses and the buses connecting the AC/DC interfacing converters (IC). The unified model is solved using the Newton-Raphson method. The extended PF equations can be used in the presence of multiple ICs operating under different control modes. Compared to other recent works, the proposed method allows multiple ICs to regulate the DC voltage simultaneously. This corresponds to more realistic operational conditions that ensure redundancy and allow for more flexible control of the hybrid grid. The proposed model can be used for networks under unbalanced conditions and allows for an intentionally negative sequence power injection. In addition to the operational advantages of this method, it is shown that the computational performance of the proposed method is one order of magnitude better than that of other methods presented in the existing recent literature while having the same accuracy.**

NOMENCLATURE

$\mathcal{N}$	Set of AC nodes
$\mathcal{M}$	Set of DC nodes
Γ	Set of IC nodes (i.e. nodes connected to the AC or DC side of the IC)
$\overline{E}$	Nodal phase-to-ground voltage phasor (AC + DC) [1]
$\bar{I}$	Current phasor (AC + DC)[1]
P	Active power
Q	Reactive power
$\overline{Y}^{ac}$	AC compound admittance matrix $\bar{I} = \overline{Y}^{ac}\overline{E}$
Y^{dc}	DC compound admittance matrix $\bar{I} = Y^{dc}\overline{E}$
I^{sw}	DC current modelling IC's switching losses
$\overline{E}^{c}$	AC voltage drop modelling IC's conduction losses
S^{loss}	Total power losses over IC
R_{eq}	Equivalent resistance of the IGBT
T_{ON}	Equivalent time constants of transistor's turn-on
T_{OFF}	Equivalent time constants of transistor's turn-off
T_{REC}	Equivalent time constants of diode's reverse recovery
$\overline{Z}^{filter}$	Impedance of the IC's filter
$\mathbf{J}$	Jacobian matrix
$\mathbf{x}$	Vector of the unknown variables
$\mathbf{y}$	Vector of the mismatches
ϵ	Convergence criteria
ν	Iteration step
$\square_i$	Subscript indicating the AC nodes
$\square_j$	Subscript indicating the DC nodes
$\square_l$	Subscript indicating IC node at the AC side
$\square_k$	Subscript indicating IC node at the DC side
$\square'$	Real part of complex number
$\square''$	Imaginary part of complex number
$\square^{\phi}$	Superscript for phase angle $\phi \in \{a, b, c\}$
$\square^{*}$	Superscript for reference point or setpoint
$\square^{0}$	Superscript indicating zero sequence
$\square^{+}$	Superscript indicating positive sequence
$\square^{-}$	Superscript indicating negative sequence

The authors are with the Swiss Federal Institute of Technology of Lausanne, Switzerland e-mail: (see willem.lambrichts@epfl.ch; mario.paolone@epfl.ch).
The project has received funding from the European Union's Horizon 2020 Research & Innovation Programme under grant agreement No. 957788.

[1] For the DC network $\Im\{\overline{E}\} = 0$ and $\Im\{\bar{I}\} = 0$

I. INTRODUCTION

Multiterminal hybrid AC/DC networks are gaining more interest nowadays in the area of HVDC as well as in hybrid AC/DC microgrids. Indeed, multiterminal HVDC systems allow the interconnection of transition networks to increase the flexibility and integration of renewables [1]. On the other hand, hybrid AC/DC microgrids are a promising solution to increase the share of distributed generation in future power grids that are expected to massively rely on converter-interfaced renewable resource generation [2].

Power flow (PF) studies are a crucial element in the analysis, planning and operation of modern power systems that are transitioning to these hybrid AC/DC systems. From a modelling point of view, the PF analysis of multiterminal HVDC systems and hybrid microgrids is identical. The main challenge comes from the incorporation of the AC/DC Interfacing Converters (IC). Indeed, the IC can operate using different control modes that affect the PF model. Typically, in a Voltage Source Converter (VSC), the d- and q-components of the current and voltages are decoupled. This allows for the control of two variables simultaneously, i.e. active power, reactive power, AC voltage, or DC voltage. The common controllable pairs of variables are: $P_{ac} - Q_{ac}$, $P_{ac} - |E_{ac}|$, $E_{dc} - Q_{ac}$ or $E_{dc} - |E_{ac}|$. For the first two operating modes, $P_{ac} - Q_{ac}$ and $P_{ac} - |E_{ac}|$, the connected AC bus is considered as a *PQ node* and *PV node*[2]. Therefore, the traditional AC power flow theory can be applied. Furthermore, using the active power balanced and IC's losses model, the DC side is modelled as a *P-node* and can be easily included in the PF model. The main challenge in the construction of a unified PF comes from the operating modes where the IC controls the DC voltage (that is, $E_{dc} - Q_{ac}$ and $E_{dc} - |E_{ac}|$). Because the DC voltage is a control variable, only one AC variable is controlled (either Q_{ac} or $|E_{ac}|$), and the traditional PF theory

[2] We use the standard PF nomenclature where in a *PV node* the active power and the voltage magnitude are controlled and in a *PQ node* the active and reactive power are controlled

cannot be used anymore. Note that at least one IC is required to control the DC voltage to ensure the stability of the DC grid.

Furthermore, hybrid AC/DC microgrids are often subjected to strong unbalanced loading conditions. Therefore, it is in the interest of the system's quality of supply to have a PF model that allows to consider generic AC unbalances including, but not limited to, the intentional injection of negative sequence power.

The structure of the paper is as follows: Section II gives a review of the state-of-the-art on PF methods for hybrid AC/DC networks and discusses several major limitations of these methods that our proposed model tackles. Section III presents the proposed generic hybrid AC/DC PF model. The load flow equations are presented for all different node types and operation modes of the ICs. Furthermore, a detailed loss model is presented that improves the accuracy of the PF solution. Section IV, presents two case studies: the first one provides a numerical validation of the proposed method on a hybrid AC/DC microgrid under balanced and unbalanced loading conditions. The second case study demonstrates the general applicability of the method for two non-synchronously connected transmission systems interfaced through two independent multiterminal HVDC networks. Section V presents an in-depth comparison and benchmark with a publicly available MATPOWER-based PF algorithm for hybrid AC/DC networks [3]. The computation time is analysed for multiple hybrid AC/DC networks, including a large network to show the scalability of our proposed method.

II. State-of-the-art review

The PF problem for AC/DC networks has been studied extensively since the 1980s. Reference [4] proposed a unified PF model that includes the DC network model and allows for a multiterminal configuration. The model is solved using the Newton-Raphson (NR) method. [5] presented a method for a decoupled PF where the ICs are modelled as voltage-dependent loads to eliminate the need for DC variables. However, these methods are only valid for Line-Commutated Converters (LCC). For VSCs, the mathematical model is fundamentally different, and the above-mentioned methods cannot be used anymore.

In the applications of VSCs, the PF models proposed in the literature can be classified into two main groups: *sequential* and *unified models*.

In the *sequential models*, the DC grid and AC grid are solved separately and iteratively linked using the active power balance at the IC that is controlling the DC voltage [6]. Notice that all, except for one, ICs are assumed to operate in PV or PQ mode. Therefore, the traditional PF theory is used to model the AC grid. The active power injection of the IC controlling the DC voltage is unknown and is computed using the active power balance between the AC and DC network. Reference [7] proposes an improved sequential PF method that includes the IC's tap positions as an additional state variable to enhance the robustness of the PF calculation.

The main problem with these methods is the need for an iterative procedure with multiple computation loops, which increases the computational complexity significantly.

In the *unified models*, the AC and DC power flows are solved as one problem by modelling the entire network (i.e., AC network, DC network and ICs) as one system.

Reference [8] proposes a unified model based on the sequential approach of [6]. The updated unified method includes the converter losses of the DC voltage-controlling IC as an optimisation variable. Using this additional variable, the active power injection on the AC side of this IC is equal to the sum of all DC power injections and losses.

The authors of [9] propose a new equivalent representation of a VSC where the converter is modelled as an ideal tap-changing transformer with a complex tap. The tap magnitude corresponds to the VSC's modulation index and the tap angle is equal to the phase angle of the AC voltage at the IC's node. An additional shunt susceptance and resistance are included to model the reactive power flow and the converter's losses. The approach allows to describe the IC's fundamental frequency operation as a two-port model. [10] includes the two-port model in a unified PF model that can handle the different operating modes and is solved using the NR method. The method requires new additional control variables and can only model the positive sequence operation of ICs.

The authors in [11], [12] propose a PF method using the Flexible Universal Branch Model (FUBM). The FUBM is based on the above-described two-port model and can realistically model AC transmission lines and VSCs operating under different operation modes. The FUBM PF-based method has been made publicly available as an extension of the MATPOWER tool and is used to benchmark our proposed method in Section V. References [13], [14] follow a similar approach in which the AC/DC IC is represented as a two-port model and is included as a building block of the compound admittance matrix of the entire AC/DC network. Therefore, the method can be integrated into conventional PF programmes with minimal modifications. Reference [15] proposes an AC-equivalent approach in which every DC line is replaced by a set of parallel AC lines and in which the ICs are replaced by an equivalent line model dependent on the modulation index.

Reference [16] proposes another method in which every IC is modelled using two conventional AC generators, one for the AC side and one for the DC side, and coupled by a linear constraint to ensure energy conservation. Furthermore, the DC network is modelled as an AC one, so existing AC-PF tools can be reused. [3]

The main limitation of all methods proposed previously in the literature is that only one IC can regulate the DC voltage. When multiple ICs regulate the voltage of the DC grid, the problem becomes unfeasible and does not converge to

[3]In the specific case where the DC voltage is regulated using droop control, references [17]–[20] propose a method where the $V_{dc} - P$ droop curves are incorporated directly into the PF model. These methods do not follow the standard PF formulation where only the active and reactive power and or the voltage (in PV nodes) are fixed.

a solution. This fundamental limitation has been identified in [8] and [11]. Having multiple ICs controlling V_{dc} is crucial for numerous reasons. 1) The security of supply of the DC system since a redundant number of converters can better keep the DC voltage within nominal bounds. Therefore, when one converter goes offline, the other converters will continue to maintain the DC voltage level. 2) When multiple converters control the DC voltage level, the power required to maintain the nominal DC voltage setpoint is shared over multiple converters. Therefore, more power can be exchanged between AC and DC networks, allowing for a broader range of operations than when only a single IC can control the DC voltage. 3) When DC/DC transformers are present, the DC grid can have multiple voltage levels, which leads to a more optimal control of the entire grid [21]. The hybrid AC/DC grid used for the validation of our proposed LF method is a real grid available at the EPFL campus that has multiple DC/DC transformers and is inspired by a real microgrid benchmark. The methods previously presented in the literature are not usable in such a network.

An additional major limitation of the methods proposed in the literature is that AC microgrids are often subjected to unbalanced loading conditions. These are created by, e.g. single-phase photovoltaic inverters or electric vehicle chargers. None of the models can handle these unbalanced conditions in the AC grid. For unbalanced DC grids, however, reference [22] has proposed a method to model bipolar lines under asymmetric DC loading conditions.

Furthermore, the above-mentioned PF models cannot account for the intentional injection of negative sequence power that is often required to compensate for the unbalanced loading conditions.

Finally, the proposed unified PF model greatly improves the computational time, in comparison to other existing PF methods for hybrid AC/DC systems.

In this respect, this paper proposes a generic method that tackles these four fundamental limitations at the same time. The method is based on the AC-PF and is suitably extended to include the DC network and the ICs. The DC network is treated as a standard AC one and the ICs are treated in a generic way. Depending on their operation mode, i.e. if a voltage or power reference is tracked, the PF equations are suitably adapted. The DC voltage control is no longer limited to only one IC. The proposed method can be used for all types of hybrid networks (i.e., multiterminal HVDC, non-synchronous AC networks interfaced via multiple DC systems or hybrid AC/DC microgrids) under balanced or unbalanced conditions. Furthermore, the method allows us to accurately model the AC/DC grid when a negative sequence power is injected to compensate for unbalances. [4].

[4]The source code is made publicly available on https://github.com/DESL-EPFL

III. Methodology

A. Node types in hybrid AC/DC networks

The PF problem requires an exact model of the AC network, the DC network, and the ICs. The AC network consists of three types of buses: *Slack*, *PV* and *PQ* nodes and is modelled using the standard PF theory. The DC network is modelled identically to the AC network with $Q = 0$ and $\overline{Z} = R$ in order to reuse the AC-PF theory. Because of the nature of the ICs, which are typically VSCs, it is not possible anymore to use the traditional PF theory and an extension is needed where the model equations are dependent on the converter's operational mode. Typically, the control architecture of VSCs allows the control of two variables simultaneously: $E_{dc}-Q_{ac}$, $P_{ac}-Q_{ac}$ and $P_{ac}-|E_{ac}|$. Tab. I gives an overview of all possible node types in hybrid AC/DC grids. Note that at least one IC is required to impose the DC voltage (E_{dc}) [8].

TABLE I: Different types of nodes in hybrid AC/DC networks and their known and unknown variables.

Bus Type	IC contrl.	Known var.	Unknown var.	Index
AC slack		$\|E_{ac}\|$, $\angle E_{ac}$	P_{ac},Q_{ac}	$s \in \mathcal{N}_{slack}$
P_{ac}, Q_{ac}		P_{ac},Q_{ac}	$\|E_{ac}\|$, $\angle E_{ac}$	$i \in \mathcal{N}_{PQ}$
P_{ac}, $\|E_{ac}\|$		P_{ac},$\|E_{ac}\|$	Q_{ac}, $\angle E_{ac}$	$i \in \mathcal{N}_{PV}$
IC_{ac}	P_{ac} - Q_{ac}	P_{ac} Q_{ac}	$\|E_{ac}\|$, $\angle E_{ac}$	$l \in \Gamma_{PQ}$
	E_{dc} - Q_{ac}	Q_{ac}	P_{ac} $\|E_{ac}\|$ $\angle E_{ac}$	$l \in \Gamma_{E_{dc}Q}$
	P_{ac} - $\|E_{ac}\|$	P_{ac} $\|E_{ac}\|$	Q_{ac} $\angle E_{ac}$	$l \in \Gamma_{PV}$
IC_{dc}	P_{ac} - Q_{ac}	P_{dc}	E_{dc}	$k \in \Gamma_{PQ}$
	E_{dc} - Q_{ac}	E_{dc}	P_{dc}	$k \in \Gamma_{E_{dc}Q}$
	P_{ac} - $\|E_{ac}\|$	P_{dc}	E_{dc}	$k \in \Gamma_{PV}$
P_{dc}		P_{dc}	E_{dc}	$j \in \mathcal{M}_P$
E_{dc}		E_{dc}	P_{dc}	$j \in \mathcal{M}_V$

B. Power flow equations

A generic hybrid AC/DC network is considered with $\mathcal{N}$ AC nodes and $\mathcal{M}$ DC nodes, where buses $(l,k) \in \Gamma$ are the couples of AC/DC converter buses (see Fig.1). Furthermore, we assume $l \in \mathcal{N}$ and $k \in \mathcal{M}$. Therefore, $(\mathcal{N} = \mathcal{N}_{slack} \cup \mathcal{N}_{PQ} \cup \mathcal{N}_{PV} \cup \Gamma_l)$ and $(\mathcal{M} = \mathcal{M}_P \cup \mathcal{M}_V \cup \Gamma_k)$

The two grids are interlinked by one or more interfacing converters (i.e., $|\Gamma| \geq 1$) that can operate under different control modes. Notice that the PF equations below are written in rectangular coordinates[5].

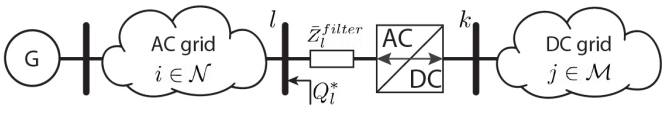

Fig. 1: The generic hybrid AC/DC network. Only one AC/DC converter is displayed for simplicity.

[5]This was a design choice by the authors, however, the model can also be easily described in polar coordinates.

1) AC network

The PF equations for *PQ* nodes read:

$$\Re\Big\{\overline{E}_i^{\phi}\sum\nolimits_{n\in\mathcal{N}}\underline{\mathbf{Y}}_{i,n}^{ac}\underline{\mathbf{E}}_n^{\phi}\Big\}=P_i^{\phi *},\quad \text{for } i\in\mathcal{N}_{PQ} \tag{1}$$

$$\Im\Big\{\overline{E}_i^{\phi}\sum\nolimits_{n\in\mathcal{N}}\underline{\mathbf{Y}}_{i,n}^{ac}\underline{\mathbf{E}}_n^{\phi}\Big\}=Q_i^{\phi *},\quad \text{for } i\in\mathcal{N}_{PQ} \tag{2}$$

The PF equations for *PV* nodes read:

$$\Re\Big\{\overline{E}_i^{\phi}\sum\nolimits_{n\in\mathcal{N}}\underline{\mathbf{Y}}_{i,n}^{ac}\underline{\mathbf{E}}_n^{\phi}\Big\}=P_i^{\phi *},\quad \text{for } i\in\mathcal{N}_{PV} \tag{3}$$

$$E_i^{\phi\prime 2}+E_i^{\phi\prime\prime 2}=E_i^{\phi *2},\quad \text{for } i\in\mathcal{N}_{PV} \tag{4}$$

where $P_i^{\phi *}$ and $Q_i^{\phi *}$ are the active and reactive power nodal injections at node i and phase $\phi\in\{a,b,c\}$. The $\square$ indicates the complex conjugate, the apostrophes $\square'$ and $\square''$ refer to the real and imaginary parts of the phase-to-ground voltage $\overline{E}_i$. $\overline{Y}^{ac}$ is the admittance matrix of the AC network.

2) DC network

The PF equations for *P* nodes in the DC grid read:

$$E_j\sum\nolimits_{m\in\mathcal{M}}Y_{j,m}^{dc}E_m=P_j^*,\quad \text{for } j\in\mathcal{M}_P \tag{5}$$

The PF equations for *V* nodes in the DC grid read:

$$E_j=E_j^*,\quad \text{for } j\in\mathcal{M}_V \tag{6}$$

3) VSC interfacing converters

For the $\mathbf{E_{dc}}-\mathbf{Q_{ac}}$ operating mode, the extended PF equations are based on the power balance (7). Notice that the reactive power losses over the filter are already accounted for in the control of the VSC (see Fig.1).

$$\begin{aligned}&P_l^a+P_l^b+P_l^c+P_{(l,k)}^{loss}+P_{(l,k)}^{filter}=P_k,\\&Q_l^a+Q_l^b+Q_l^c-Q_{(l,k)}^{loss}=Q_l^*,\qquad \text{for } (l,k)\in\Gamma_{E_{dc}Q}\end{aligned} \tag{7}$$

with Q_l^* the reactive power setpoint of the VSC and subscripts $\square_k$ and $\square_l$ referring to the resp. DC and AC side of the VSC. In a balanced system, the power is shared equally among the three phases, and thus $P_l^{\phi}=\frac{1}{3}P_k$ and $Q_l^{\phi}=\frac{1}{3}Q_l^*$. In unbalanced systems, the phase-locked loop (PLL) usually synchronizes to the AC network positive sequence, therefore, only the positive sequence powers are injected:

$$\begin{cases}P_l^0 &=0\\ P_l^+ &+P_{(l,k)}^{+loss}+P_{(l,k)}^{+filter}=P_k\\ P_l^- &=0\end{cases}$$

$$\begin{cases}Q_l^0 &=0\\ Q_l^+ &-Q_{(l,k)}^{+loss}=Q_l^*\\ Q_l^- &=0\end{cases} \tag{8}$$

where

$$P_l^+ = \Re\Big\{\overline{E}_l^+\sum\nolimits_{n\in\mathcal{N}}\underline{\mathbf{Y}}_{(l,n)}^{ac}\underline{\mathbf{E}}_n^+\Big\}, \tag{9}$$

$$Q_l^+ = \Im\Big\{\overline{E}_l^+\sum\nolimits_{n\in\mathcal{N}}\underline{\mathbf{Y}}_{(l,n)}^{ac}\underline{\mathbf{E}}_n^+\Big\}, \tag{10}$$

$$P_k^+ = \Re\Big\{E_k^*\sum\nolimits_{m\in\mathcal{M}}Y_{(k,m)}^{dc}E_m\Big\} \tag{11}$$

and E_k^* is the DC voltage setpoint.

Because $\overline{S}_l^0=P_l^0+jQ_l^0=\overline{E}_l^0\underline{\mathbf{I}}_l^0$, the homopolar component of the voltage E_l^0, or the current I_l^0, has to be zero. For a VSC, where the voltage is controlled, E_l^0 is set to zero. For a current source converter, I_l^0 would be zero (idem for the negative sequence component). Note here that this operation distinction has to be made, since the expression for the homopolar and negative sequence powers in (8) cannot be used. Using these power injections results in a trivial expression, and thus in an underdetermined problem.

Substituting expressions (9), (10) and (11) into (8) reads:

$$\begin{cases}E^{0\prime}=0\\ \Re\Big\{\overline{E}_l^+\sum_{n\in\mathcal{N}}\underline{\mathbf{Y}}_{(l,n)}^{ac}\underline{\mathbf{E}}_n^+\Big\}+P_{(l,k)}^{+loss}+P_{(l,k)}^{+filter}=\\ \qquad\qquad E_k^*\left(Y_{(k,k)}^{dc}E_k^*+\sum_{m\neq k}^{m\in\mathcal{M}}Y_{(k,m)}^{dc}E_m\right)\\ E^{-\prime}=0\end{cases} \tag{12}$$

$$\begin{cases}E^{0\prime\prime}=0\\ \Im\Big\{\overline{E}_l^+\sum_{n\in\mathcal{N}}\underline{\mathbf{Y}}_{(l,n)}^{ac}\underline{\mathbf{E}}_n^+\Big\}-Q_{(l,k)}^{+loss}=Q_l^*\\ E^{-\prime\prime}=0\end{cases} \tag{13}$$

Rewriting the positive sequence component of (12) to E_k^* (the controllable DC voltage) leads to the quadratic equation (14):

$$\begin{aligned}\Big(Y_{(k,k)}^{dc}\Big)E_k^{*2}+\Big(\sum\nolimits_{m\neq k}^{m\in\mathcal{M}}Y_{(k,m)}^{dc}E_m\Big)E_k^*\\ -\Re\Big\{\overline{E}_l^+\sum\nolimits_{n\in\mathcal{N}}\underline{\mathbf{Y}}_{(l,n)}^{ac}\underline{\mathbf{E}}_n^+\Big\}=0\end{aligned} \tag{14}$$

Solving the quadratic equation (14) to E_k^* results in two solutions: one close to 1 p.u. and another (infeasible) close to 0 p.u. Because the operational voltage of a grid is close to 1 p.u., the only feasible solution is given by the positive equation (15).

$$E_k^*=-\frac{\sum_{m\neq k}^{m\in\mathcal{M}}Y_{(k,m)}^{dc}E_m}{2Y_{(k,k)}^{dc}}\pm \frac{\sqrt{\left(\sum_{m\neq k}^{m\in\mathcal{M}}Y_{(k,m)}^{dc}E_m\right)^2-4Y_{(k,k)}^{dc}\Re\Big\{\overline{E}_l^+\sum_{n\in\mathcal{N}}\underline{\mathbf{Y}}_{(l,n)}^{ac}\underline{\mathbf{E}}_n^+\Big\}}}{2Y_{(k,k)}^{dc}} \tag{15}$$

Notice that (15) is dependent on the AC positive sequence nodal voltage component $\overline{E}^+$. Using the standard Fortescue symmetrical component decomposition, the nodal voltage can be transformed back to the phase domain:

$$\begin{bmatrix}\overline{E}^0\\ \overline{E}^+\\ \overline{E}^-\end{bmatrix}=\frac{1}{3}\begin{bmatrix}1&1&1\\ 1&\overline{\alpha}&\overline{\alpha}^2\\ 1&\overline{\alpha}^2&\overline{\alpha}\end{bmatrix}\cdot\begin{bmatrix}\overline{E}^a\\ \overline{E}^b\\ \overline{E}^c\end{bmatrix} \tag{16}$$

For the $\mathbf{P_{ac}}-\mathbf{Q_{ac}}$ operating mode, the AC side of a generic VSC, which can inject positive and negative power references, is modelled as (17) and (18). In the case that the IC only injects the positive sequence, the power balance of the negative sequence is replaced by $\overline{E}^-=0$.

$$\begin{cases} E^{0\prime} = 0 \\ \Re\Big\{ \overline{E}_l^{+} \sum_{n\in\mathcal{N}} \underline{\mathbf{Y}}_{(l,n)}^{ac} \underline{\mathbf{E}}_n^{+} \Big\} - P_{(l,k)}^{+loss} = P_l^{+*} \\ \Re\Big\{ \overline{E}_l^{-} \sum_{n\in\mathcal{N}} \underline{\mathbf{Y}}_{(l,n)}^{ac} \underline{\mathbf{E}}_n^{-} \Big\} - P_{(l,k)}^{-loss} = P_l^{-*} \end{cases} \tag{17}$$

$$\begin{cases} E^{0\prime\prime} = 0 \\ \Im\Big\{ \overline{E}_l^{+} \sum_{n\in\mathcal{N}} \underline{\mathbf{Y}}_{(l,n)}^{ac} \underline{\mathbf{E}}_n^{+} \Big\} - Q_{(l,k)}^{+loss} = Q_l^{+*} \\ \Im\Big\{ \overline{E}_l^{-} \sum_{n\in\mathcal{N}} \underline{\mathbf{Y}}_{(l,n)}^{ac} \underline{\mathbf{E}}_n^{-} \Big\} - Q_{(l,k)}^{-loss} = Q_l^{-*}, \end{cases} \quad \text{for } (l,k) \in \Gamma_{PQ} \tag{18}$$

The active power balance also imposes the DC power injection on the DC side. Taking the converter and filter losses into account gives:

$$P_l^{*} \quad = E_k \sum\nolimits_{m\in\mathcal{M}} Y_{k,m}^{dc} E_m - P_{(l,k)}^{loss} - P_{(l,k)}^{filter} \tag{19}$$

For the $\mathbf{P_{ac}} - |\mathbf{E_{ac}}|$ operating mode, the interfacing VSC model consists of equations (8) and (4).

C. AC/DC interfacing converter loss model

The losses of the AC/DC interfacing converter can be included for a more accurate grid model. Assuming that the semiconductor switches of the VSCs are Insulated-Gate Bipolar Transistors (IGBT), references [23], [24] propose an accurate VSC loss model. The converter model that includes the losses and filter is shown in Fig.2. The conduction losses are modelled as a voltage source $\overline{E}_l^c$ on the AC side (20) and the switching losses as a DC current source I_k^{sw} (21).

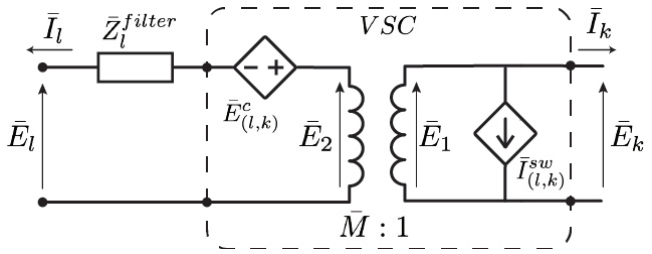

Fig. 2: Transformer-like model of an inverter leg of the AC/DC interfacing converter with RL filter.

$$\overline{E}_{(l,k)}^c = R_{eq}\left(|\bar{I}_l|\right)\bar{I}_l \tag{20}$$

$$\bar{I}_{(l,k)}^{sw} = 2\frac{T_{ON}+T_{OFF}+T_{REC}}{T_s}\ \frac{1}{N}\cot(\frac{\pi}{N})|\bar{I}_l| \tag{21}$$

where R_{eq} is the equivalent resistance of the IGBT, T_s is the switching period, and $N = {}^{f_s}/_{f_{grid}}$ is the ratio between the converter's switching frequency and the grid frequency. T_{ON} and T_{OFF} are the equivalent time commutation constants characterising the transistor's turn-on and turn-off effects under the test conditions, and T_{REC} is the reverse recovery at turn-off of the diode. It can be observed that the losses, $\overline{E}_l^c$ and I_k^{sw}, are only dependent on the converter's switching frequency and the several parameters that can be easily derived from the semiconductor's datasheet.

The total losses are computed as the sum of the conduction and switching losses:

$$\overline{S}_{(l,k)}^{loss} = \overline{E}_{(l,k)}^c \sum\nolimits_{n\in\mathcal{N}} \underline{Y}_{(l,n)}^{ac} \underline{E}_n + I_{(l,k)}^{sw} E_k \tag{22}$$

In the application of HVDC, typically the IC's losses are modelled using a quadratic expression that accounts for the current dependent losses and the constant losses, such as active cooling and auxiliary equipment [25], [26].

$$P_{(l,k)}^{loss} = a + b|\bar{I}_l| + c|\bar{I}_l|^2, \tag{23}$$

where a (in W) represents the no-load losses of the transformer and the average loss of the auxiliary equipment. b (in $\mathrm{W\,A^{-1}}$) represents the switching loss of the switches and the diodes and c (in Ω) represents the conduction losses of the switches [25]. Reference [26] shows typical values for the losses in a HVDC VSC station. Compared to the loss model in (22), this quadratic expression includes the constant losses that can be beneficial in the application of HVDC where auxiliary equipment is present. As shown later, either (22) or (23) can be used to model the IC's losses.

The active losses over the *RL*-filter with impedance $\overline{Z}_l^{filter}$ can be straightforwardly modelled as:

$$P_{(l,k)}^{filter} = \Re\Big\{ \overline{Z}_l^{filter} \Big| \sum\nolimits_{n\in\mathcal{N}} \overline{Y}_{(l,n)}^{ac} \overline{E}_n \Big|^2 \Big\} \tag{24}$$

As known, any filter, i.e. with or without shunt capacitive elements, can always be represented as a passive and reciprocal two-port model. Therefore, a unique PI-equivalent model can be derived and added to the systems admittance matrix.

D. Solution via the Newton-Raphson method

The PF problem given by (1)-(4), (5), (6) (12), (13), the positive solution of (15), (17) and (18) is solved in a unified way via the Newton-Raphson (NR) method. In compact matrix formulation, it can be written as:

$$\mathbf{J}^{(\nu)} \cdot \Delta\mathbf{x}^{(\nu+1)} = \Delta\mathbf{y}^{(\nu)} \tag{25}$$

where

$$\Delta\mathbf{x}^{(\nu+1)} = \mathbf{x}^{(\nu+1)} - \mathbf{x}^{(\nu)} \tag{26}$$

$$\Delta\mathbf{y}^{(\nu)} = \mathbf{y}^{*} - F(\mathbf{x}^{(\nu)}) \tag{27}$$

where ν is the iteration step, $\mathbf{J}$ is the PF Jacobian composed by the first-order partial derivatives of the PF model, $\mathbf{x}$ is the vector of the unknown variables. $\Delta\mathbf{y}$ is the mismatch related to the known variables, i.e., the difference between the power or voltage setpoint, indicated by the symbol $*$, and the evaluated PF equations. For the hybrid system discussed in the case study in Section IV, the linearised system of equations gives:

$$\begin{bmatrix} J_{P_{ac}/E'} & J_{P_{ac}/E''} & J_{P_{ac}/E_{dc}} \\ J_{Q_{ac}/E'} & J_{Q_{ac}/E''} & J_{Q_{ac}/E_{dc}} \\ \hdashline J_{E_{dc}/E'} & J_{E_{dc}/E''} & J_{E_{dc}/E_{dc}} \\ J_{P_{ac}^{+}/E'} & J_{P_{ac}^{+}/E''} & J_{P_{ac}^{+}/E_{dc}} \\ J_{Q_{ac}^{+}/E'} & J_{Q_{ac}^{+}/E''} & J_{Q_{ac}^{+}/E_{dc}} \\ \hdashline J_{E_{ac}^{0\prime}/E'} & J_{E_{ac}^{0\prime}/E''} & J_{E_{ac}^{0\prime}/E_{dc}} \\ J_{E_{ac}^{-\prime}/E'} & J_{E_{ac}^{-\prime}/E''} & J_{E_{ac}^{-\prime}/E_{dc}} \\ J_{E_{ac}^{0\prime\prime}/E'} & J_{E_{ac}^{0\prime\prime}/E''} & J_{E_{ac}^{0\prime\prime}/E_{dc}} \\ J_{E_{ac}^{-\prime\prime}/E'} & J_{E_{ac}^{-\prime\prime}/E''} & J_{E_{ac}^{-\prime\prime}/E_{dc}} \\ \hdashline J_{P_{dc}/E'} & J_{P_{dc}/E''} & J_{P_{dc}/E_{dc}} \end{bmatrix} \cdot \begin{bmatrix} \Delta E' \\ \Delta E'' \\ \Delta E_{dc} \end{bmatrix} = \begin{bmatrix} \Delta P_{ac} \\ \Delta Q_{ac} \\ \hdashline \Delta E_{dc} \\ \Delta P_{ac}^{+} \\ \Delta Q_{ac}^{+} \\ \hdashline \Delta E_{ac}^{0\prime} \\ \Delta E_{ac}^{-\prime} \\ \Delta E_{ac}^{0\prime\prime} \\ \Delta E_{ac}^{-\prime\prime} \\ \hdashline \Delta P_{dc} \end{bmatrix} \tag{28}$$

where e.g. $J_{P_{ac}/E'}$ is the partial derivative $\frac{\partial P_{ac}}{\partial E'}$.

The unknowns are updated at each step by taking the inverse of the Jacobian until the convergence criterium is reached.

$$\mathbf{x}^{(\nu+1)} = \mathbf{x}^{(\nu)} + \mathbf{J}^{(\nu)^{-1}} \Delta \mathbf{y}^{(\nu)} \tag{29}$$

The convergence criterium is set on the update of the mismatches (30) where ϵ is the desired tolerance:

$$\Delta \mathbf{y}^{(\nu)} < \epsilon \tag{30}$$

E. Integration of IC constraints in the PF model

The proposed PF method can take the operational limits of the ICs into account by means of a suitable adaptation. The method used here follows a similar logic as the standard AC-constrained PF as described, for instance, in [27]. This is only relevant when two or more converters are present to regulate the DC voltage or the AC voltage: i.e. operating mode $\mathbf{E_{dc}} - \mathbf{Q_{ac}}$ or $\mathbf{P_{ac}} - |\mathbf{E_{ac}}|$. This can be explained as follows: when two or more converters regulate the voltage, the power that is required to obtain the desired DC and/or AC voltage can be shared over multiple converters. Therefore, when the solution of the PF methods shows that one converter is exceeding its operation limits, the other converters could increase their supply to ensure the PQ capability of the limiting converter is satisfied again. Therefore, we can solve another load flow where the operation mode of the converter that has reached its operational limits is changed to $\mathbf{P_{ac}} - \mathbf{Q_{ac}}$. The active or reactive power, depending on what is the limiting variable, is set to its maximum value. Next, the load flow is solved again until all converters are operating within their PQ capability curves[6]. The flowchart of the NR algorithm for the unified PF of hybrid AC/DC networks is shown in Figure 3

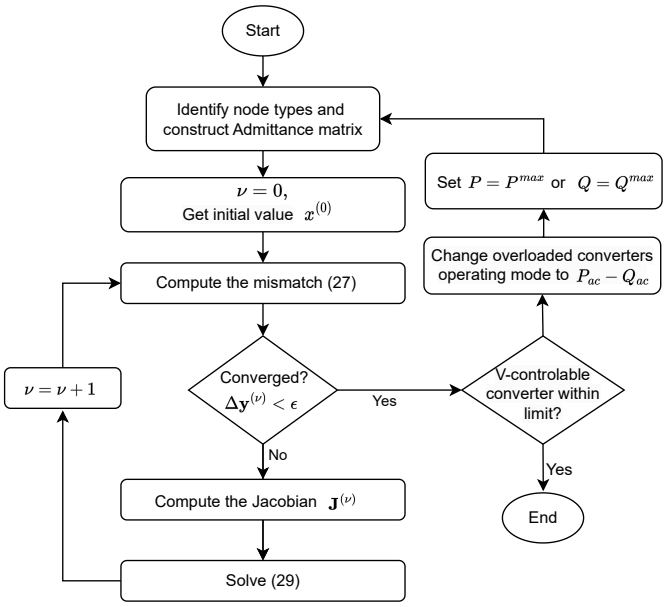

Fig. 3: Flow chart of the NR algorithm for the unified and constrained PF of hybrid AC/DC networks.

[6]In the case only one voltage-regulating converter is present, and the active or reactive power limit is exceeded, the power cannot be shared among another converter. Therefore, the load-flow solution will not be within the feasible operation limits and the operator knows that it is not possible to operate the grid without exceeding its limitations.

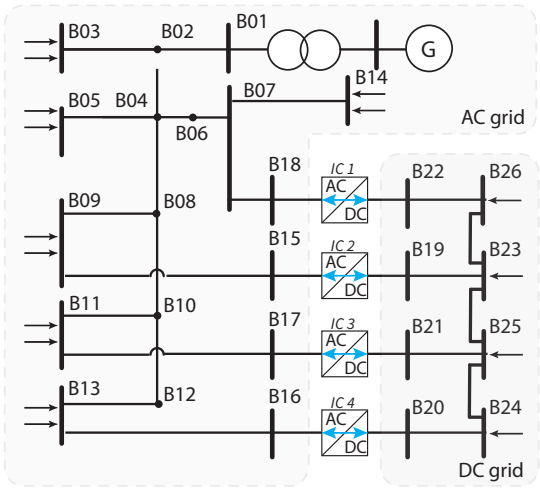

Fig. 4: Topology of the hybrid AC/DC microgrid developed at the EPFL

IV. Case Study

A. Hybrid AC/DC microgrid

The proposed PF algorithm for hybrid AC/DC is first validated on the hybrid AC/DC microgrid developed at the EPFL. The topology and parameters of the hybrid network are presented in [28] and shown in Fig. 4. The hybrid AC/DC microgrid consists of 18 AC nodes, 8 DC nodes, and 4 interfacing converters that can work under two control modes: $\mathbf{E_{dc}} - \mathbf{Q_{ac}}$ and $\mathbf{P_{ac}} - \mathbf{Q_{ac}}$. Tab. II summarises the node types in the hybrid network. Both grids have a base power of $100\,\mathrm{kVA}$ and a base voltage of $400\,\mathrm{V_{ac}}$ and $800\,\mathrm{V_{dc}}$. Notice that any method previously proposed in the literature cannot be used for the PF analysis of this hybrid microgrid because two IC are controlling the DC voltage. The model is made publically available to the interested reader to reproduce the results at https://github.com/DESL-EPFL.

TABLE II: Node types in the hybrid AC/DC microgrid

AC	
Bus Type	**Bus #**
PQ	2-14
IC ($E_{dc} - Q_{ac}$)	16,18
IC (P_{ac} - Q_{ac})	15,17
AC slack	1

DC	
Bus Type	**Bus #**
P	24-26
IC ($E_{dc} - Q_{ac}$)	20,22
IC (P_{ac} - Q_{ac})	19,21

Two steady-state time simulations are performed in the EMTP-RV simulation environment: a balanced one and a strongly unbalanced one, where the difference power injections between the phases in *B09* reaches 0.5 p.u. The results from the simulation are considered the 'ground truth' and are used to validate the PF algorithm. The active and power injections are taken from real operating conditions that have been observed in the hybrid microgrid available at the Distributed Electrical Systems Laboratory of the EPFL [29]. The NR convergence criterium (30) is set at $\epsilon < 10^{-6}$ for the update of the mismatches $\Delta \mathbf{y}$. The voltage errors, the difference between the ground truth and the results of the load flow algorithm, are presented as a histogram in Fig.5. The top figures show the voltage errors of the real and imaginary components and

TABLE III: Maximum and mean errors between the true state and load flow results for balanced and unbalanced operating conditions (in p.u.)

Case	Grid	Nodal voltage		Current injection		Line losses	
		Mean	Max	Mean	Max	Mean	Max
Bal.	**AC**	2.76e-6	7.36e-6	5.28e-6	4.55e-5	3.55e-7	3.03e-6
	DC	1.54e-8	5.88e-8	2.33e-7	3.30e-7	5.60e-10	1.74e-9
Unbal.	**AC**	9.31e-6	2.03e-5	2.00e-5	1.72e-4	1.08e-6	7.76e-6
	DC	8.19e-8	2.59e-7	5.40e-7	1.49e-6	5.69e-10	3.97e-9

the DC voltages for the balanced case. The results of the unbalanced case are shown in the two lower figures. For the balanced loading conditions, the maximum voltage error is in the order of 1×10^{-6}. For the unbalanced loading conditions, the maximum error is in the order of 1×10^{-5}. The maximum and mean errors on the nodal voltages, current injections and losses for the AC and DC grid are summarized in Table III for the balanced and unbalanced cases.

The NR algorithm takes around 20 ms and 4 iterations to converge for the considered three-phase 26-node hybrid microgrid when starting from a *flat start* where the voltage magnitudes are initialised at 1 p.u. The numerical experiment has been performed on a 2020 Apple Macbook Pro with an Intel Quad-Core i7 processor and 32 GB of RAM

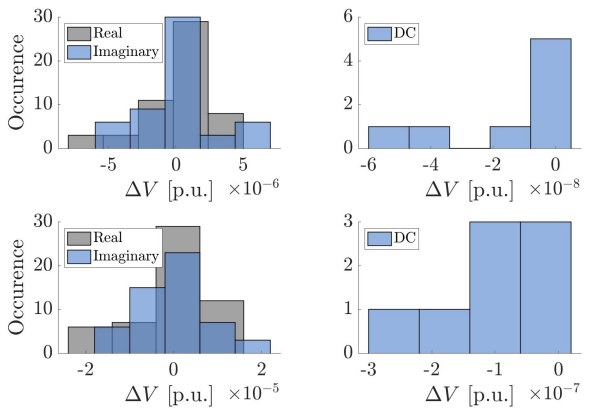

Fig. 5: Histogram of the voltage errors between the true state and load flow results. Top - balanced case, bottom - unbalanced case. Left - AC grid, right - DC grid.

Furthermore, the proposed PF model is validated on the hybrid microgrid for a wide range of operating scenarios via a dedicated Monte Carlo analysis. The analysis is presented in Appendix A. Additionally, Appendix A also presents a loadability assessment of the ICs and the AC and DC nodes.

B. Multiterminal HVDC network

The proposed PF model is here applied to study the PF in a multiterminal HVDC grid that interconnects two non-synchronous AC networks, see Figure (6). The hybrid grid's topology has been originally proposed in [19]. The two AC grids are the IEEE 57-bus and IEEE 14-bus reference networks. The IEEE 57 bus system supplies 42 loads through 80 lines with 7 generators and the IEEE 14 bus system supplies 11 loads through 20 lines with 5 generators. Both AC systems have a base voltage of 100 kV and a base power of 100 MVA. The AC networks are interfaced using two separate HVDC networks. HVDC system #1 consists of 7 nodes, 7 lines and hosts a wind park generating 10 MVA. HVDC system #2 consists of 3 nodes and 3 lines. Both DC grids have a base voltage of 200 kV and a base power of 100 MVA. The IC loss model is the quadratic model as in (23). The loss models parameters are selected according to typical values that are reported in references [26], [30], i.e. $a = 0.011$, $b = 0.0034$ and $c = 0.011$ p.u.. Furthermore, the operational conditions of the AC and DC networks are summarised in Table VI. The generation and load of all the individual nodes, and the network topology and parameters are available on the DESL GitHub page [7].

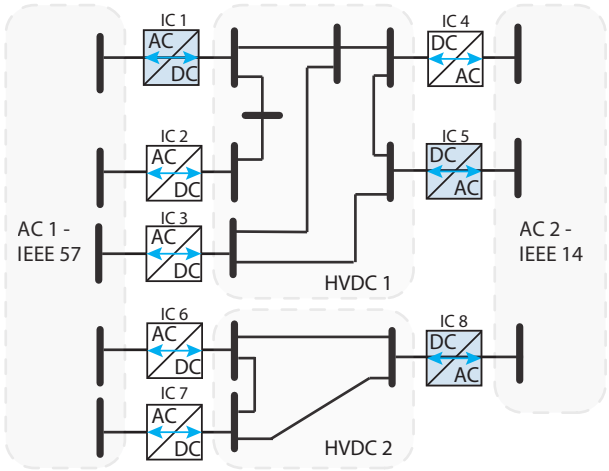

Fig. 6: Two non-synchronous AC grids interlinked by two HVDC grids. The interfacing converters in blue regulate the DC voltage

Because the two AC grids are not synchronous, each network requires a slack bus to set the voltage magnitude and angle in at least one node. Furthermore, to demonstrate the generality of the proposed method, two interfacing converters regulate the DC voltage in HVDC grid 1 (highlighted in blue in Figure 6). The results of the PF are shown in Table IV. Because of space limitations, only the relevant results, i.e. powers, voltages and losses of the interfacing converters, are shown. It is shown that the two voltage-regulating converters share the power required to set the DC voltage. Therefore, each voltage-regulating converter station is less loaded and the voltage profiles in the DC network are closer to their nominal value.

TABLE IV: Results of the proposed PF model for the two non-synchronous grids interlinked by two HVDC grids (in p.u.)

HVDC	IC #	Control mode	P_{ac}	Q_{ac}	$\lvert V_{ac}\rvert$	V_{dc}	P^{losses}
1	**1**	$\mathbf{E_{dc} - Q_{ac}}$	-0.56	**-0.05**	0.932	**1.000**	17.2e-3
	2	$\mathbf{P_{ac} - Q_{ac}}$	-0.38	**-0.15**	0.996	**1.000**	14.2e-3
	3	$\mathbf{P_{ac} - Q_{ac}}$	**0.45**	**0.30**	0.992	0.985	16.2e-3
	4	$\mathbf{P_{ac} - Q_{ac}}$	**0.15**	**-0.40**	0.965	0.990	14.7e-3
	5	$\mathbf{E_{dc} - Q_{ac}}$	**0.15**	**0.50**	1.009	0.991	15.8e-3
2	**6**	$\mathbf{P_{ac} - Q_{ac}}$	-0.34	**0.11**	0.961	**1.000**	13.7e-3
	7	$\mathbf{P_{ac} - Q_{ac}}$	**0.20**	**0.21**	0.946	0.992	13.1e-3
	8	$\mathbf{E_{dc} - Q_{ac}}$	**0.10**	**-0.31**	0.943	0.993	13.5e-3

[7] https://github.com/DESL-EPFL

TABLE V: Operational conditions of AC system: total generation, load and losses (active and reactive power in p.u.)

	Total gen.		Total load		Total losses	
AC grid	**P**	**Q**	**P**	**Q**	**P**	**Q**
IEEE 57	10.18	6.58	-8.90	-2.91	1.28	3.67
IEEE 14	3.82	2.20	-3.52	-1.24	0.30	0.97

TABLE VI: Operational conditions of DC system: total generation, load and losses (active power in p.u.).

HVDC	**Total gen.**	**Total load**	**Total losses**
1	0.90	-0.89	-11.5e-3
2	0.33	-0.32	-2.4e-3

C. Integration of IC constraints in the PF model

The integration of the IC constraints, discussed in Section III-E, is demonstrated here. We use the multiterminal HVDC network introduced above and assume that all the ICs have an active power limit of ± 0.5 p.u.

As highlighted in Table IV, the active power injection of *IC 1* equals -0.56 p.u. and exceeds the converters' active power limit of -0.5 p.u. Because *IC 1* and *IC 2* are both operating in voltage control mode, the active power injections can be shared among both converters to reduce the power injection of the *IC 1*. Therefore, using the constrained PF method presented in the flow chart in Figure 3, the operation mode of *IC 1* is changed to $\mathbf{P_{ac}} - \mathbf{Q_{ac}}$. Additionally, its active power setpoint is set to the maximum: $P_{ac} = -0.5$ p.u.

Next, the PF is recomputed and the results are shown in Table VII. We can see that *IC 2* increased its power injection from -0.38 p.u. to -0.43 p.u. to reduce the active power injection of *IC 1*. All the ICs are now operating within their limits.

TABLE VII: Results of the proposed constrained PF model for the two non-synchronous grids interlinked by two HVDC grids (in p.u.)

HVDC	**IC #**	**Control mode**	P_{ac}	Q_{ac}	$\lvert V_{ac}\rvert$	V_{dc}	P^{losses}
	1	$\mathbf{E_{dc}} - \mathbf{Q_{ac}}$	**-0.50**	**-0.05**	0.949	0.997	15.9e-3
	2	$\mathbf{P_{ac}} - \mathbf{Q_{ac}}$	-0.43	**-0.15**	0.995	**1.000**	15.1e-3
1	**3**	$\mathbf{P_{ac}} - \mathbf{Q_{ac}}$	**0.45**	**0.30**	0.995	0.982	16.2e-3
	4	$\mathbf{P_{ac}} - \mathbf{Q_{ac}}$	**0.15**	**-0.40**	0.965	0.990	14.7e-3
	5	$\mathbf{E_{dc}} - \mathbf{Q_{ac}}$	**0.15**	**0.50**	1.009	0.991	15.8e-3
	6	$\mathbf{P_{ac}} - \mathbf{Q_{ac}}$	-0.34	**0.11**	0.961	**1.000**	13.7e-3
2	**7**	$\mathbf{P_{ac}} - \mathbf{Q_{ac}}$	**0.20**	**0.21**	0.946	0.992	13.1e-3
	8	$\mathbf{E_{dc}} - \mathbf{Q_{ac}}$	**0.10**	**-0.31**	0.943	0.993	13.5e-3

V. Comparison with existing methods

The performance of the proposed method is also benchmarked against the FUBM-based PF algorithm proposed in [11], [12]. The PF model has been made publicly available as an extension of the MATPOWER package [3]. As discussed in Section II, the model is based on the universal branch model to model the ICs and requires four additional state variables to model each AC-DC interface: two variables (m_a and θ_a) to model the amplitude modulation and the phase-shifting action of the PWM control of the VSC, a shunt susceptance B_{eq} to compensate the reactive power injected into the DC grid and the variable G^{sw}, accounting for the VSC losses. The PF model is solved using the Newton-Raphson method.

The comparison is performed on four different hybrid AC/DC networks: 1) the hybrid microgrid developed at the EPFL presented in Section IV, 2) the IEEE 30-node transmission system that has been extended with a 3 and 5-node DC network, 3) the IEEE 57-node network that is connected to the IEEE 14-node network using a DC network, also shown in Figure 6, and 4) the modified 1354-node PEGASE network to showcase the scalability of our proposed method. The modifications made on the IEEE networks and the PEGASE network to include a DC system, have been proposed by [11].

The FUBM-based PF algorithm only works for balanced, single-phase systems (i.e. only the direct sequence equivalent is considered) and, furthermore, the method is limited to only one IC to control the DC voltage. Therefore, our proposed model has been appropriately adapted to consider only the direct sequence, and the studied networks only contain one voltage-controllable IC.

The two PF methods are compared in accuracy and computation time. To allow a fair comparison, the boundary conditions are set the same: the power setpoints of all the generators and loads, the type of nodes (*PV* or *PQ*) and the operating modes of the ICs. The convergence criteria (30) for both methods are set at $\epsilon < 10^{-8}$ for the update of the mismatches. Furthermore, the initial conditions of the unknowns, $\mathbf{x}^{(0)}$, are all set at $1p.u.$.

The results of the time analysis for the four reference hybrid AC/DC networks are presented in Table VIII. The CPU time (in seconds), the number of state variables, and the number of iterations required to reach the convergence criteria are shown. To allow a fair comparison, only the time to run the iterative NR process is considered, i.e., the computation of the mismatch equations, the construction of the Jacobian and the update of the unknowns. The columns *EPFL* indicate the results of our proposed PF methods, while *FUBM* refers to the results of the FUBM method presented in [11].

It can be seen that the computation time of the proposed method is one order of magnitude smaller than the FUBM method. This can be explained by the fact that the FUBM requires additional variables to model the ICs. Therefore, the number of unknowns increases along with the number of iterations and consequently, the computation time. The method proposed in this paper does not require additional variables to model the IC's behaviour since it is an extension of the AC-PF and only requires 2 variables for each AC node and 1 variable for each DC node. The large CPU time of the FUBM method is mainly due to the computation of the partial derivatives of the power injections with respect to the variables m_a and B_{eq} which are needed for the IC's model.

The scalability of the method is demonstrated on the 1354-node PEGASE grid. Despite the large number of unknowns, the proposed method can solve the PF in 6 iterations in the order of seconds. The number of state variables is this time lower in the FUBM model. This is because the FUBM model is formulated in polar coordinates, and a large number of generators (261) are present in the PEGASE grid. The

generators are modelled as PV nodes and because of the polar representation of the FUBM method, only one state variable per *PV node* is needed. Our proposed method is formulated in rectangular coordinates and requires 2 state variables per PV node.

TABLE VIII: Comparison of the computational time of our proposed method *(prop.)* with different PF methods.

	CPU time [s]		# iterations		# states	
	Prop.	FUBM	Prop.	FUBM	Prop.	FUBM
μ Grid (Sec. IV)	0.018	0.515	4	11	41	60
IEEE 30	0.023	0.412	4	5	82	109
IEEE 57+14	0.035	0.469	4	5	174	200
PEGASE	2.533	13.75	6	7	2724	2490

VI. Conclusion

In this paper, we present a novel model for the power flow in multiterminal hybrid AC/DC networks. The model is formulated in a general and unified way and solved using the Newton-Rapson method. New to previously published works, the proposed methodology allows multiple AC/DC converters to control the DC voltage. This is a crucial element in the planning and control of multiterminal AC/DC networks, as it corresponds more to the realistic operational condition of these hybrid grids. Additionally, the model is able to compute the power flow under balanced and unbalanced loading conditions and can account for intentionally negative sequence power injection.

The method is numerically validated on a hybrid AC/DC microgrid, whose topology has been inspired by a real benchmark grid. Multiple ICs regulate the DC voltage level and the network is subjected to unbalanced loading conditions. It is shown that the error between the ground truth, obtained in an EMTP-RV time-domain simulation, and the results of the proposed PF method exhibits a maximum error of 1×10^{-6} p.u. for the nodal voltages and 1×10^{-5} p.u. for the current injections. A Monte Carlo analysis is presented where the proposed method is validated for a wide range of realistic operating scenarios for the load demand and ICs. Additionally, a loadability assessment of the ICs and the AC and DC nodes is presented.

Furthermore, the generality of the PF method is demonstrated for a transmission system that consists of two non-synchronous grids, coupled through two meshed HVDC networks.

Finally, the computational time of the proposed method is compared with the FUBM-based PF method, which is implemented as an extension of the MATPOWER tool. The comparison has been performed using multiple hybrid networks with different voltage levels, topologies, and sizes. The convergence criterion is set the same for both methods. It is shown that the method proposed in this paper converges by a factor of 10 faster than the FUBM-based method.

Appendix A
Monte Carlo analysis

A Monte Carlo analysis is performed to show the applicability of the proposed PF for a wide range of operating conditions of a targeted AC/DC hybrid grid. The analysis is performed on the direct-phase equivalent of the 26-node hybrid AC/DC microgrid (see Section IV). The scenarios are generated based on realistic operating limits of the resources that are hosted at the experimental hybrid AC/DC network available at the EPFL. The operating limits of the resources in the AC network, and DC network, and the power and voltage limits of the ICs are summarized in Table IX.

TABLE IX: The operating limits of the resources for the AC network, DC network and the interfacing converters

AC resources

Bus #	Active power	Reactive power	Voltage
3	$[0, 30]$ kW	$[-30, 30]$ $kVAr$	/
5	$[-25, 25]$ kW	$[-25, 25]$ $kVAr$	/
9	$[-110, 120]$ kW	$[-110, 110]$ $kVAr$	/
11	$[0, 30]$ kW	$[-0, 0]$ $kVAr$	/
13	$[-5, 15]$ kW	$[0, 0]$ $kVAr$	/
14	$[-30, 30]$ kW	$[-30, 30]$ $kVAr$	/

DC resources

Bus #	Active power	Reactive power	Voltage
23	$[-10, 15]$ kW	/	/
24	$[0, 5]$ kW	/	/
25	$[0, 5]$ kW	/	/
26	$[0, 5]$ kW	/	/

Interfacing converters

Bus #	Active power	Reactive power	Voltage
IC1	/	$[-45, 45]$ $kVAr$	$[760, 840]$ V_{dc}
IC2	$[-45, 45]$ kW	$[-45, 45]$ $kVAr$	/
IC3	$[-45, 45]$ kW	$[-45, 45]$ $kVAr$	/
IC4	/	$[-45, 45]$ $kVAr$	$[760, 840]$ V_{dc}

Given the operational limits of the resources listed in Table IX, we suppose that each power (active and reactive) and voltage setpoint in each node is uniformly distributed within these bounds. $10\,000$ scenarios are generated assuming the above distributions are independent and identically distributed (i.i.d.). The results are represented in Figure 7 as boxplots regarding the AC/DC nodal voltage magnitudes. The blue boxes indicate the 75% quantile and the outliers are shown in the dashed line. The proposed method exhibits remarkable convergence properties since it is able to compute the solution of the PF in each of the scenarios and with very few iterations (5 to 6 iterations).

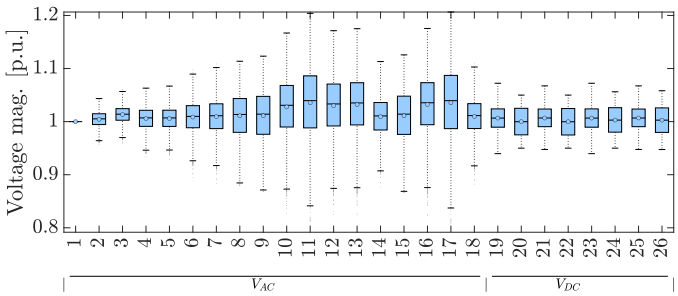

Fig. 7: Boxplot of the distribution of the voltage magnitudes of the Monte Carlo analysis. The horizontal axis represents every node in the AC and DC network

Loadability assessments

In a loadability assessment, the PF solution is computed when the active and reactive load of an individual node

or IC are gradually increased until the PF becomes unfeasible/unsolvable. In figure 8a and 8b, we quantify the voltage trajectories in the IC's AC node *B15* when the active and reactive power setpoints of the IC2 increase (between *B15* and *B19*). In Figure 8c and 8d, the loadability curves of the *B14* (a PQ-node) are shown, where the active power and reactive power load at the same node (*B14*) gradually increase. Figure 8e shows the voltage profile of *B26* (a P-node) where the DC power load at the same node gradually increases.

These figures show how the method is capable of inferring the loadability curves of the considered network over a wide range of possible operating conditions of the ICs and the load demands in the AC and DC network and demonstrate the validity of the proposed PF model for all these scenarios.

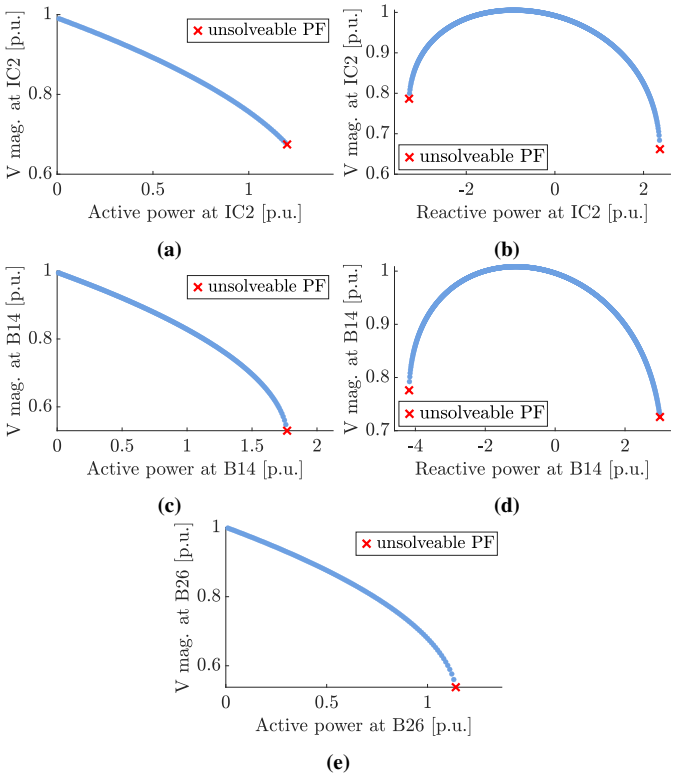

Fig. 8: Loadability curves of the active and reactive power for individual nodes in the AC grid, DC grid and interfacing converter.

REFERENCES

[1] ENTSO-E, "Hvdc links in system operations," Available: https://eepublicdownloads.entsoe.eu/ (accessed in August 2023), Tech. Rep., December 2019.

[2] N. Eghtedarpour and E. Farjah, "Power control and management in a hybrid ac/dc microgrid," *IEEE transactions on smart grid*, vol. 5, no. 3, pp. 1494–1505, 2014.

[3] R. D. Zimmerman, C. E. Murillo-Sánchez, and R. J. Thomas, "Matpower: Steady-state operations, planning, and analysis tools for power systems research and education," *IEEE Transactions on power systems*, vol. 26, no. 1, pp. 12–19, 2011.

[4] D. A. Braunagel, L. A. Kraft, and J. L. Whysong, "Inclusion of dc converter and transmission equations directly in a newton power flow," *IEEE Transactions on Power Apparatus and Systems*, vol. 95, no. 1, pp. 76–88, 1976.

[5] T. Smed, G. Andersson, G. Sheble, and L. Grigsby, "A new approach to ac/dc power flow," *IEEE Transactions on Power Systems*, vol. 6, no. 3, pp. 1238–1244, 1991.

[6] J. Beerten, S. Cole, and R. Belmans, "A sequential ac/dc power flow algorithm for networks containing multi-terminal vsc hvdc systems," in *IEEE PES general meeting*. IEEE, 2010, pp. 1–7.

[7] C. Liu, B. Zhang, Y. Hou, F. F. Wu, and Y. Liu, "An improved approach for ac-dc power flow calculation with multi-infeed dc systems," *IEEE Transactions on Power Systems*, vol. 26, no. 2, pp. 862–869, 2010.

[8] M. Baradar, M. Ghandhari, and D. Van Hertem, "The modeling multi-terminal vsc-hvdc in power flow calculation using unified methodology," in *2011 2nd IEEE ISGT*. IEEE, 2011, pp. 1–6.

[9] E. Acha, B. Kazemtabrizi, and L. M. Castro, "A new vsc-hvdc model for power flows using the newton-raphson method," *IEEE Transactions on Power Systems*, vol. 28, no. 3, pp. 2602–2612, 2013.

[10] E. Acha and L. M. Castro, "A generalized frame of reference for the incorporation of, multi-terminal vsc-hvdc systems in power flow solutions," *Electric Power Systems Research*, vol. 136, pp. 415–424, 2016.

[11] A. Alvarez-Bustos, "Flexible universal branch model for steady state operational analysis and optimisation of hybrid ac/dc grids," Ph.D. dissertation, Durham University, 2021.

[12] A. Alvarez-Bustos, B. Kazemtabrizi, M. Shahbazi, and E. Acha-Daza, "Universal branch model for the solution of optimal power flows in hybrid ac/dc grids," *International Journal of Electrical Power & Energy Systems*, vol. 126, p. 106543, 2021.

[13] M. M. Rezvani and S. Mehraeen, "Unified ac-dc load flow via an alternate ac-equivalent circuit," *IEEE Transactions on Industry Applications*, vol. 57, no. 6, pp. 5626–5635, 2021.

[14] ——, "A generalized model for unified ac-dc load flow analysis," in *2021 IEEE Texas Power and Energy Conference*. IEEE, 2021, pp. 1–6.

[15] A. Kumar and T. Ghose, "A newton-raphson-based unified load flow of grid-connected and islanded ac–dc microgrids," *I. Transactions on Electrical Energy Systems*, vol. 31, no. 11, p. e13075, 2021.

[16] J. Renedo, A. A. Ibrahim, B. Kazemtabrizi, A. Garcia-Cerrada, L. Rouco, Q. Zhao, and J. Garcia-Gonzalez, "A simplified algorithm to solve optimal power flows in hybrid vsc-based ac/dc systems," *International Journal of Electrical Power & Energy Systems*, vol. 110, pp. 781–794, 2019.

[17] E. Aprilia *et al.*, "Unified power flow algorithm for standalone ac/dc hybrid microgrids," *IEEE Transactions on smart grid*, vol. 10, no. 1, pp. 639–649, 2017.

[18] Q. Nguyen, G. Todeschini, and S. Santoso, "Power flow in a multi-frequency hvac and hvdc system: Formulation, solution, and validation," *IEEE TPS*, vol. 34, no. 4, pp. 2487–2497, 2019.

[19] R. Chai *et al.*, "Unified power flow algorithm based on the nr method for hybrid ac/dc grids incorporating vscs," *IEEE Transactions on Power Systems*, vol. 31, no. 6, pp. 4310–4318, 2016.

[20] A. Eajal *et al.*, "A unified approach to the power flow analysis of ac/dc hybrid microgrids," *IEEE Transactions on sustainable energy*, vol. 7, no. 3, pp. 1145–1158, 2016.

[21] R. P. Barcelos and D. Dujić, "Direct current transformer impact on the dc power distribution networks," *IEEE Transactions on Smart Grid*, vol. 13, no. 4, pp. 2547–2556, 2022.

[22] L. Mackay, R. Guarnotta, A. Dimou, G. Morales-España, L. Ramirez-Elizondo, and P. Bauer, "Optimal power flow for unbalanced bipolar dc distribution grids," *IEEE Access*, vol. 6, pp. 5199–5207, 2018.

[23] F. Scapino, "A transformer-like model for the dc/ac converter," in *IEEE ICIT, 2003*, vol. 1. IEEE, 2003, pp. 625–630.

[24] F. Scapino , "Vsi lossy models for circuit simulation including high-impedance state," in *Proc. of the IEEE ISIE*, vol. 2, 2005, pp. 565–570.

[25] H. Ergun, J. Dave, D. Van Hertem, and F. Geth, "Optimal power flow for ac–dc grids: Formulation, convex relaxation, linear approximation, and implementation," *IEEE transactions on power systems*, vol. 34, no. 4, pp. 2980–2990, 2019.

[26] G. Daelemans, K. Srivastava, M. Reza, S. Cole, and R. Belmans, "Minimization of steady-state losses in meshed networks using vsc hvdc," in *2009 IEEE Power & Energy Society General Meeting*. IEEE, 2009, pp. 1–5.

[27] B. Stott, "Review of load-flow calculation methods," *Proceedings of the IEEE*, vol. 62, no. 7, pp. 916–929, 1974.

[28] W. Lambrichts and M. Paolone, "Linear recursive state estimation of hybrid and unbalanced ac/dc micro-grids using synchronized measurements," *IEEE Transactions on Smart Grid*, 2022.

[29] ——, "Experimental validation of a unified and linear state estimation method for hybrid ac/dc microgrids," in *2023 IEEE Belgrade PowerTech*. IEEE, 2023, pp. 1–8.

[30] J. Beerten, S. Cole, and R. Belmans, "Generalized steady-state vsc mtdc model for sequential ac/dc power flow algorithms," *IEEE Transactions on Power Systems*, vol. 27, no. 2, pp. 821–829, 2012.

Willem Lambrichts received the B.Sc. degree in electrical engineering from the Catholic University of Leuven, Belgium in 2018 and the M.Sc in energy engineering from the Catholic University of Leuven in 2020. Since 2020, he has been pursuing his PhD degree at the Distributed Electrical Systems Laboratory, EPFL, Switzerland. His research interests include state estimation and optimal grid-aware control in the domain of hybrid AC/DC distribution networks.

Mario Paolone (M'07, SM'10, F'22) received the M.Sc. (Hons.) and Ph.D. degrees in electrical engineering from the University of Bologna, Italy, in 1998 and 2002. In 2005, he was an Assistant Professor in power systems at the University of Bologna, where he was with the Power Systems Laboratory until 2011. Since 2011, he has been with the Swiss Federal Institute of Technology, Lausanne, Switzerland, where he is a Full Professor and the Chair of the Distributed Electrical Systems Laboratory. His research interests focus on power systems with particular reference to real-time monitoring and operational aspects, power system protections, dynamics and transients. Dr Paolone's most significant contributions are in the field of PMU-based situational awareness of Active Distribution Networks (ADNs) and in the field of exact, convex and computationally efficient methods for the optimal planning and operation of ADNs. Dr. Paolone was the founder and Editor-in-Chief of the Elsevier journal Sustainable Energy, Grids and Networks.